

ELECTRON CLOUD DENSITY MEASUREMENTS USING RESONANT MICROWAVES AT CESRTA*

J.P. Sikora[†], CLASSE, Ithaca, New York 14853 USA
S. De Santis, LBNL, Berkeley, California 94720 USA

Abstract

Hardware has recently been installed in the Cornell Electron Storage Ring (CESR) to extend the capability of resonant microwave measurement of electron cloud density. Two new detector locations include aluminum beam-pipe in a dipole magnet and copper beam-pipe in a field free region. Measurements with both positron and electron beams are presented with both beams showing saturation of the electron cloud density in the aluminum chamber. These measurements were made at CESR which has been reconfigured as a test accelerator (CESRTA) with positron or electron beam energies ranging from 2 GeV to 5 GeV.

INTRODUCTION

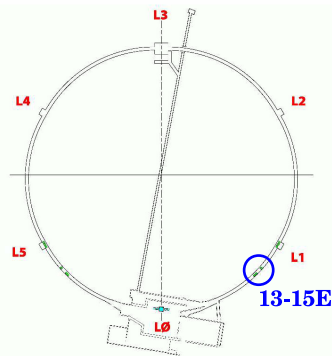


Figure 1: This sketch of the CESR storage ring shows the location of the 13-15E region where the the new measurement hardware is installed.

The Cornell Electron Storage Ring (CESR) has a circumference of 768 m and supports positron or electron beams with bunch populations of up to 1.6×10^{11} particles/bunch (10 mA/bunch) with total beam populations of 3.8×10^{12} particles/beam. Beam energies range from roughly 2 GeV to 5 GeV. The CESR test accelerator program (CESRTA) includes the study of the build-up and decay of electron cloud (EC) density [1], which in this storage ring is dominated by the photo-electrons that are produced by synchrotron radiation. A number of techniques have been used to measure EC density at different locations in CESR [2], including microwave measurements.

To use microwaves for EC density measurements, the microwaves are coupled into and out of the beam-pipe as

*This work is supported by the US National Science Foundation PHY-0734867, PHY-1002467 and the US Department of Energy DE-FC02-08ER41538, DE-SC0006505.

[†]jps13@cornell.edu

described in Ref. [3] and shown in Fig. 2, typically using electrodes designed for the beam position monitor (BPM) system. If the response of the beam-pipe is resonant, the presence of the electron cloud will shift the resonant frequency slightly as given in Eq. 1 where n_e is the local EC density and E the local electric field of the microwaves, ϵ_0 is the vacuum permittivity, e is the charge and m_e the mass of an electron. The integral is taken over the resonant volume V of the section of beam-pipe. If the beam-pipe is excited at a fixed frequency near resonance and the electron cloud is periodic, as with a train of bunches in a storage ring, the result is modulation sidebands above and below the excitation frequency. The EC density can be calculated from the amplitude of the sidebands as described in Ref. [3]. This technique is also referred to as the resonant TE wave method [4, 5, 6].

$$\frac{\Delta\omega}{\omega_0} \approx \frac{e^2}{2\epsilon_0 m_e \omega_0^2} \frac{\int_V n_e E_0^2 dV}{\int_V E_0^2 dV} \quad (1)$$

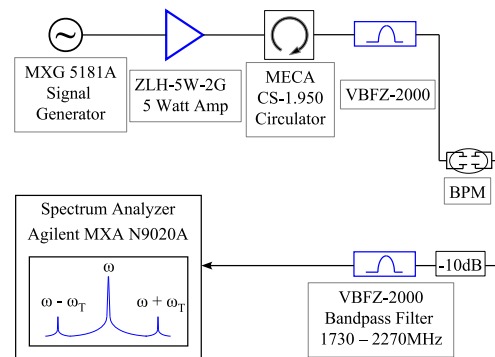


Figure 2: The hardware provides a drive signal to excite the beam-pipe at near a resonant frequency. The response will be phase modulated by the periodic EC density.

HARDWARE

The instrumentation needed to make the measurement is a signal generator and a 5 W amplifier to provide the drive and a spectrum analyzer to measure the sideband amplitudes. Filters and a circulator are also used to protect the instruments from the signal produced by the beam. We have recently added a set of high bandwidth relays that will allow the remote selection of three locations for connection to the drive and receive instruments during accelerator operation. Similar connections have already been made in other parts of the storage ring [7].

Microwaves are routed to and from the BPM electrodes at the three locations using low loss Andrew LDF4-50A coaxial cable and coaxial relays as shown in Fig. 3. The relays are Dynatek model 06-133k10 coaxial switches that were part of the original beam position monitor system in CESR.

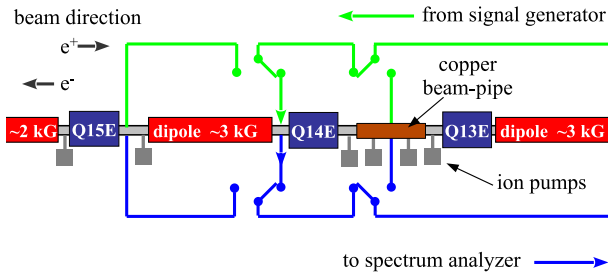


Figure 3: Microwaves are routed to and from three detectors in the storage ring using low-loss cable and rf relays.

Standing Wave Patterns

Microwave resonances are generated by changes in the beam-pipe geometry that produce reflections of the microwaves, especially near the cutoff frequency of the beam-pipe. Known reflectors of microwaves are the longitudinal slots that connect ion pumps to the beam vacuum space in the aluminum chamber of the CESR ring. Figure 4 shows some of the relevant dimensions of the 13-15E section of beam-pipe, including the locations of the ion pumps. Also shown is a copper test chamber in the straight section between Q13E and Q14E.

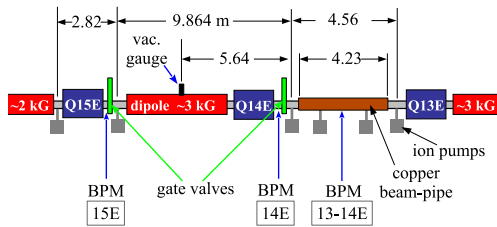


Figure 4: Sketch of the 13-15E section of beam-pipe with some dimensions. The BPMs used to couple microwaves in/out of the beam-pipe are labelled.

Figure 5 shows the response at the section between 13-14E. In this case, the resonances follow the expected $f^2 = f_c^2 + (nc/2L)^2$ pattern of a waveguide with its ends shorted having a cutoff frequency f_c and a length L with n the number of half wavelengths in the standing wave. Matching the measured response to the expected response gives a cutoff frequency f_c of 1.756 GHz for the copper beam-pipe with a length L of 4.23 m. This length is very close to the measured distance between transitions in the beam-pipe from the copper to the aluminum chamber. The aluminum beam-pipe in CESR is made from an extrusion whose cutoff frequency has been determined to be 1.896 GHz by similar measurements made in another part of the storage ring.

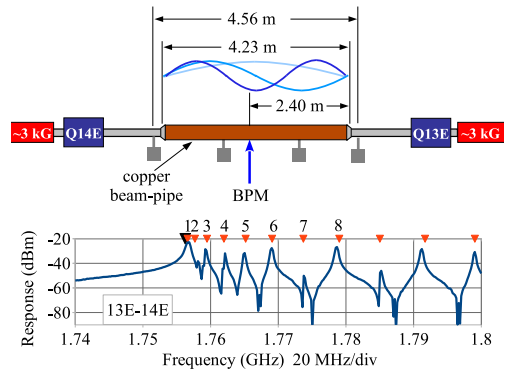


Figure 5: The response of the 13-14E section of beam-pipe has a series of resonances that are consistent with a shorted waveguide having a cutoff frequency of 1.756 GHz and a length of 4.23 m, matching the dimensions of the copper chamber. The calculated frequencies are shown as triangles with the larger dark triangle the cutoff frequency f_c .

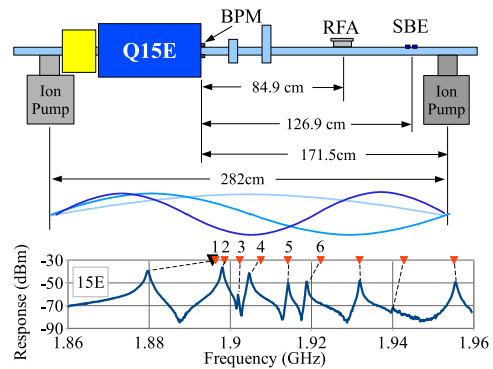


Figure 6: The response of the 15E section of beam-pipe shows frequencies similar to that of a shorted waveguide. The expected values are shown as triangles with dotted lines connecting them to possible corresponding peaks. The dark triangle is the cutoff frequency.

Figure 6 shows the response at the section that includes 15E. In this case the response is similar to the response expected from a shorted section of waveguide, but there are some notable differences. Since this section is constructed with a standard CESR aluminum extrusion, the cutoff frequency is taken to be 1.896 GHz. Using the 2.82 m distance between the ion pumps as the length of the resonant section, the expected resonant frequencies are plotted as triangles in Fig. 6. The lowest resonance is well below the cutoff frequency and several of the resonances are below the predicted values. A conjecture is that the gate valve near the middle of this section of beam-pipe and close to the drive point has a strong influence on the resonant series. The inner dimensions of the valve are somewhat wider than the beam-pipe to prevent synchrotron radiation from striking the valve body directly. This wider dimension lowers the cutoff frequency within the valve and can result in a resonance below the cutoff frequency of the surrounding beam-

pipe. For frequencies above cutoff, this larger volume at the gate valve will lower the frequency of any resonance that has significant field at that longitudinal position.

Figure 7 shows the response when driving the BPM at 14E. Using the known cutoff frequency of the aluminum extrusion, the plot also shows the expected resonances using two different lengths: 9.86 m is the distance between the nearest ion pumps and 5.64 m is the distance from the ion pump nearest to the drive point to a vacuum gauge port in the middle of the dipole. Neither of these lengths gives a reasonable match to the measured response. As in the case of 15E, the lowest resonance is below the cutoff frequency, probably due to the influence of the nearby gate valve. Further modeling, or special measurements will be needed in order to understand the nature of the standing waves in this section.

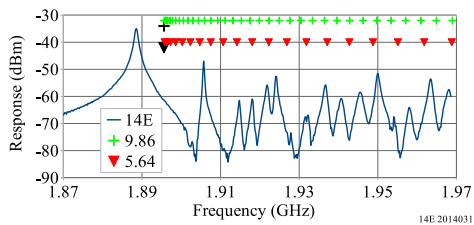


Figure 7: The response of the 14E section of beam-pipe does not match well the model of a shorted section of waveguide. Triangles show the location of resonances that might be expected with the given beam-pipe geometry.

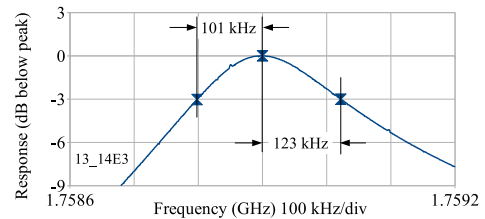


Figure 8: This detail of the response of the 13E-14E section of beam-pipe shows the asymmetry of the second resonance.

Table 1: Q Values for Beam-pipe Resonances

Resonance	f_0 (GHz)	$\pm\Delta f$ (kHz)	Q
13-14E1	1.7563150	-285/250	3277
13-14E2	1.7588850	-101/123	7852
13-14E3	1.7617530	-83/95	9897
13-14E4	1.7646210	-95/105	8824
13-14E5	1.7686440	-118/129	7132
13-14E6	1.7782610	-148/144	6089
14E1	1.88822	-438/440	2146
14E2	1.90535	-144/147	6571
15E1	1.879351	-358/342	2686
15E2	1.897685	-215/200	4584
15E3	1.90430	-176/187	5261
15E4	1.91390	-153/164	6057
15E5	1.91847	-133/171	6312

Calibration

Several auxiliary measurements are needed in order to obtain a calibration of the EC density for a given sideband amplitude: the Q of the resonances, an estimate of the time development of the periodic EC density as well as estimates of the uniformity of the EC density over the resonant volume. For a given maximum EC density, the sideband amplitudes will be determined by the envelope of the changing EC density vs. time and the Q of each resonance. Also, since the microwave resonance extends over some length of beam-pipe and the EC density can change over that length, it is important to understand the effect that this change in density has on the measurement.

The Q of a resonance can be obtained by measuring the frequency difference Δf between the resonance peak f_0 and where the response is lower by 3 dB. Then $Q = f_0 / (2\Delta f)$. Figure 8 shows the response of a particular resonance where the value of Δf is not the same above and below the resonant frequency. This is presumably due to the presence of nearby resonances that make the response asymmetric. Our present analysis does not take this into account; the average of the upper and lower values of Δf is used. Table 1 shows the measured -3 dB points and the corresponding Qs for the different resonances.

With a fixed drive frequency near resonance, the periodic EC density will produce phase modulation sidebands

whose amplitudes are given by the EC density's time structure. The periodic EC density versus time is convolved with the response time of the resonance ($\tau = 2Q/\omega_0$), when calculating the periodic phase. The simplest approximation is to begin with a rectangular EC density, which has a fixed value for the duration of the bunch train and is zero otherwise. This approximation has given normalized sideband amplitudes that are about 10% higher when compared with the shape given by ECLLOUD simulations [8]. For the measurements discussed in this paper, only the first sidebands of each resonance will be used, assuming the rectangular approximation in the calculation of the EC density.

Equation 1 shows that if the EC density n_e is uniform over the resonant volume, the shift in frequency $\Delta\omega/\omega$ will be proportional to that uniform density. If the EC density varies over the volume, the meaning of the calculated value will need some interpretation. Figure 9 shows the effect that an EC density $n_e(s)$ that changes with the position s has on the quantity $n_e(s)E_0^2(s)$. In this case, we set $E_0(s)$ to be a half sine wave over the resonant length L . The frequency shift $\Delta\omega$ will be proportional to the integral of the resulting curve.

It can be shown that a linear change in EC density from one end of the resonant section to the other gives the following result: the magnitude of the frequency shift $\Delta\omega$ will correspond to the EC density at the midpoint of the

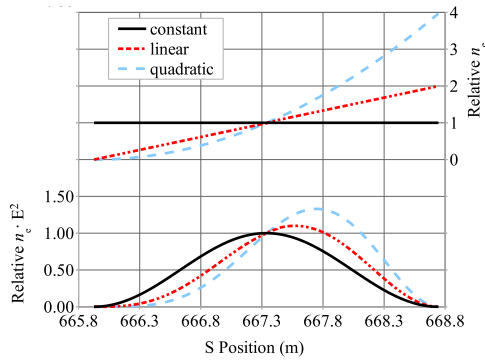


Figure 9: An EC density that changes over the length of the resonant section will change the local value of $n_e(s)E_0^2(s)$.

resonance length, as if that density were uniform over the volume. If the change in EC density is non-linear over the resonance length, the corresponding frequency shift would have to be calculated by integrating Eq. 1. This effect is shown in Fig. 9.

In the CESR storage ring, the source of cloud electrons is almost exclusively from photo-electrons. So we make the approximation that the EC density is proportional to the photon rate at each location along the resonant length. This ignores, for example, the effect that magnetic fields will have on EC density. Figure 10 shows the relative photon rates at 13-14E for both positrons and electrons along with the span of the resonant section and its center.

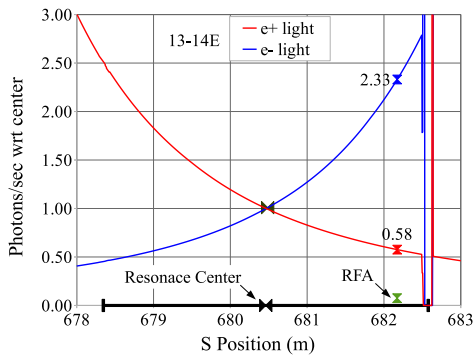


Figure 10: Estimates of the relative photon rates from positrons and electrons are show versus position in the section from 13-14E, normalized to the rate at the resonance center. Also shown is the location and rates at a retarding field analyzer (RFA) in the same section of beam-pipe.

DATA

Data was taken with 5.3 GeV beams of 20 bunches spaced by 14 ns for both positrons and electrons. The analysis of the data uses the rectangular approximation for the EC density, having a length of 266 ns with a revolution period of 2562 ns. The Q values are taken from Table 1. The EC density is taken to be proportional to the local photon

rate and the normalized integral – using the relative photon rates as in Fig. 10 – is used to calculate a correction to the EC density and obtain the value at the center of the resonant length. This correction is made for each resonance and is different for positrons and electrons since the synchrotron light distribution is different. For the 15E data, the corrections are between 3% and 10%; for the 13-14E data, the corrections vary from 6% to 18% due to the higher non-linearity of the EC density. For 14E, since the standing wave pattern is not understood, a correction for a varying EC density was not made.

Data from the 13E-14E Section

Data from the 13-14E section with a positron beam is shown in Fig.11 for six resonances in the copper chamber. There is a roughly 30% range of values for EC density, depending on the resonance used. If $E_0^2(s)$ of the resonance is symmetric, the measurements at each resonance should give the same result provided that the change in EC density along the length of the resonance has been compensated correctly.

The result with an electron beam is shown in Fig.12, where the EC density is generally lower than for positrons. For both positrons and electrons, the EC density increases roughly linearly with beam current.

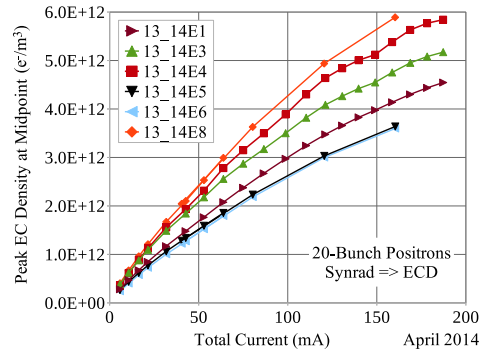


Figure 11: Data taken at 13-14E with a positron beam using six different resonances.

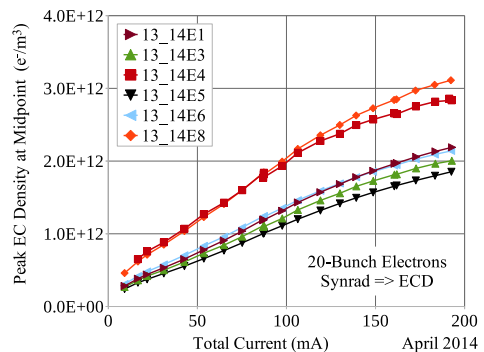


Figure 12: Data taken at 13-14E with an electron beam using six different resonances.

Data from the 14E Section

At 14E, data was taken using only the two lowest resonances, with both positron and electron data appearing in Fig.13. The electron data shows an interesting curvature at the lowest currents and all of the data appears to saturate with higher currents. In this case, the EC density obtained from the two resonances is different by a factor of two for both the positron and electron beams. This data has not been corrected for a varying EC density over its resonant length, since the resonant length is not known. Further work is required to understand data from this section.

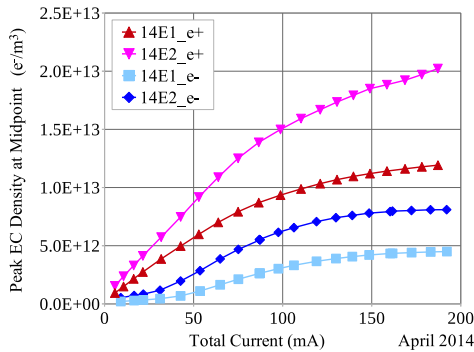


Figure 13: Data take at 14E with both positrons and electrons using the two lowest peaks of Fig.7.

Data from the 15E Section

At 15E, data was taken using five resonances of Fig. 6. The positron data in Fig.14 shows saturation at higher beam currents and a variation of about 25% between values of EC density obtained by the different resonances. The electron data of Fig.15 shows varying degrees of saturation.

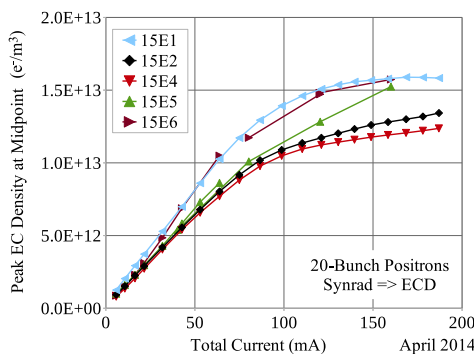


Figure 14: Positron data taken at 15E using five resonances.

CONCLUSIONS

A new section of the CESR ring has been instrumented so that EC density data can be taken at three different drive/receive points using the resonant microwave method.

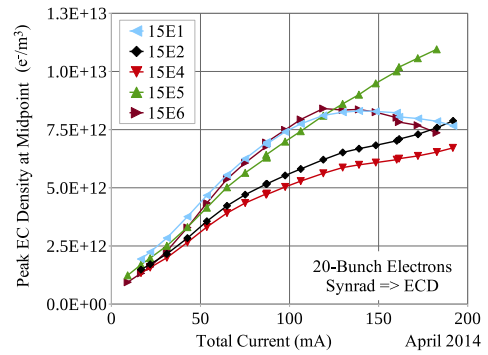


Figure 15: Electron data taken at 15E using five resonances.

Corrections have been made in the calibration through approximate Q measurements and an estimate of the variation in the EC density along the resonant length. A better understanding of the standing wave patterns is needed, especially at 14E. The data obtained also have a number of features that need further explanation, including variations in the measured density with different resonances in the same chamber.

REFERENCES

- [1] G.F. Dugan, *et al.*, ICFA Beam Dynamics Newsletter No. 50, J. Urakawa and W. Chou, Eds. (2009).
- [2] “The CESRTA: Phase I Report,” Tech. Rep. CLNS-12-2084, LEPP, Cornell University, Ithaca, NY (Jan. 2013). <http://www.lns.cornell.edu/public/CLNS/2012/>
- [3] J.P. Sikora, *et al.*, Nucl. Instrum. Methods Phys. Res., Sect. A **754**, pp. 28-35 (2014), <http://dx.doi.org/10.1016/j.nima.2014.03.063>, Preprint, arXiv:1311.5633 [physics.acc-ph].
- [4] J. P. Sikora, *et al.*, “Resonant TE Wave Measurements of Electron Cloud Densities at CESRTA,” in Proc. of IPAC’11, San Sebastián, Spain, August 2011, TUPC170, p.1434, (2011).
- [5] J. P. Sikora, *et al.*, “TE Wave Measurement and Modeling,” in *Proceedings of ECLLOUD 2012, La Biodola, Elba, Italy*, edited by R. Cimino, G. Rumolo, F. Zimmermann, CERN-2013-002, CERN, Geneva, Switzerland, 2013, p. 193-200, arXiv:1307.4315 [physics.acc-ph].
- [6] J.P. Sikora, *et al.*, “Resonant TE Wave Measurement of Electron Cloud Density Using Multiple Sidebands”, in Proc. of IBIC’13, Oxford, United Kingdom, September 2013, TUPF34, (2013).
- [7] J. P. Sikora, S. De Santis, K. Hammond, “TE Wave measurements at CESRTA,” in *Proceedings of ECLLOUD 2010, Ithaca, NY*, edited by Karl Smolenski, Cornell University, Ithaca, NY, 2013, p. 95-99.
- [8] J.P. Sikora, *et al.*, “Cross-calibration of Three Electron Cloud Density Detectors at CESRTA,” *these proceedings*, THCB1, IBIC’14, Monterey, CA, USA, (2014).